

# Bubble Coalescence during Acoustic Cavitation in Aqueous Electrolyte Solutions

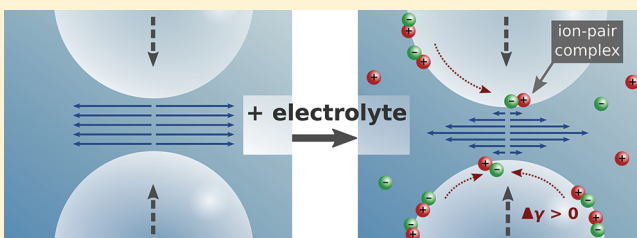
Christine Browne,<sup>†,‡</sup> Rico F. Tabor,<sup>†,§</sup> Derek Y. C. Chan,<sup>†,||,⊥</sup> Raymond R. Dagastine,<sup>†,§</sup> Muthupandian Ashokkumar,<sup>†,‡</sup> and Franz Grieser<sup>\*,†,‡</sup>

<sup>†</sup>Particulate Fluids Processing Centre, <sup>‡</sup>School of Chemistry, <sup>§</sup>Department of Chemical and Biomolecular Engineering, and <sup>||</sup>Department of Mathematics and Statistics, The University of Melbourne, Parkville, Victoria 3010 Australia

<sup>⊥</sup>Faculty of Life and Social Sciences, Swinburne University of Technology, Hawthorn, Victoria 3122 Australia

**ABSTRACT:** Bubble coalescence behavior in aqueous electrolyte (MgSO<sub>4</sub>, NaCl, KCl, HCl, H<sub>2</sub>SO<sub>4</sub>) solutions exposed to an ultrasound field (213 kHz) has been examined. The extent of coalescence was found to be dependent on electrolyte type and concentration, and could be directly linked to the amount of solubilized gas (He, Ar, air) in solution for the conditions used. No evidence of specific ion effects in acoustic bubble coalescence was found. The results have been compared with several previous coalescence studies on bubbles in aqueous electrolyte

and aliphatic alcohol solutions in the absence of an ultrasound field. It is concluded that the impedance of bubble coalescence by electrolytes observed in a number of studies is the result of dynamic processes involving several key steps. First, ions (or more likely, ion-pairs) are required to adsorb at the gas/solution interface, a process that takes longer than 0.5 ms and probably fractions of a second. At a sufficient interfacial loading (estimated to be less than 1–2% monolayer coverage) of the adsorbed species, the hydrodynamic boundary condition at the bubble/solution interface switches from tangentially mobile (with zero shear stress) to tangentially immobile, commensurate with that of a solid–liquid interface. This condition is the result of spatially nonuniform coverage of the surface by solute molecules and the ensuing generation of surface tension gradients. This change reduces the film drainage rate between interacting bubbles, thereby reducing the relative rate of bubble coalescence. We have identified this point of immobilization of tangential interfacial fluid flow with the “critical transition concentration” that has been widely observed for electrolytes and nonelectrolytes. We also present arguments to support the speculation that in aqueous electrolyte solutions the adsorbed surface species responsible for the immobilization of the interface is an ion-pair complex.



## INTRODUCTION

The effect of solutes, in particular electrolytes, on bubble coalescence behavior in water and other solvents has been the subject of considerable scrutiny over a sustained period of time. Of particular interest has been the intriguing observation of coalescence inhibition, or not in some cases, that electrolytes appear to impress on both multibubble (in bubble swarms) and isolated two-bubble interactions.<sup>1–8</sup> For electrolytes that are able to inhibit bubble coalescence, a “critical transition concentration” has been identified, representing the electrolyte concentration at which a 50% reduction in the coalescence rate of bubbles in pure water occurs. To date, there has been no convincing qualitative understanding, let alone a theoretical predictive model developed, that can adequately explain the coalescence inhibition/noninhibition phenomenon exacted by electrolytes.<sup>9,10</sup>

In the most recent experimental study<sup>8</sup> that attempts to establish a basis for the electrolyte coalescence inhibitory effect, the authors speculate that it stems from a specific ion affinity for the bubble–solution interface. Henry and Craig<sup>8</sup> have hypothesized that the presence of ions (actually cation–anion couples) at the gas–solution interface, together with an inherent kilohertz oscillatory undulation of the interface, gives rise to nonequilibrium surface tension gradients. It is the effect of these concentration

gradients that are mooted to reduce the film drainage rate between colliding bubbles and hence inhibit the rate of bubble–bubble coalescence.

The irradiation of a liquid with ultrasound also produces bubbles but with characteristics that differ considerably from bubbles under “silent” conditions. Bubbles exposed to ultrasound (or to sound in general) experience quite dynamic physical conditions.<sup>11</sup> The oscillatory pressure gradients produced by a sound field passing through a liquid cause bubbles to oscillate, grow in size, move rapidly through a liquid with speeds<sup>12</sup> of up to 1.6 m/s, and to aggregate into clusters or “bubble clouds”.<sup>11</sup> Some bubbles may also violently implode, producing transient “hot spots” with temperatures peaking at several thousand degrees, and as such give rise to sonoluminescence and sonochemistry.<sup>13</sup>

Several studies on acoustic bubbles have shown an inhibition effect of solutes, particularly surface-active solutes, on the net coalescence occurring in a multibubble system exposed to ultrasound.<sup>14–16</sup> Very similar trends have been observed to those reported in “standard” two-bubble and multibubble coalescence

Received: July 21, 2011

Revised: August 22, 2011

Published: August 25, 2011

studies. For example, the critical transition concentration, in both method types, is reduced as the alkyl chain length of a homologous series of aliphatic alcohols is increased.<sup>3,14,15</sup> Also, low levels of surfactants (<1 mM) similarly inhibit coalescence in acoustic<sup>14,15</sup> and nonacoustic coalescence systems.<sup>3</sup>

There are, however, several significant differences between acoustic bubbles and the bubbles typically used to study bubble coalescence. Acoustic bubbles are considerably smaller (a few micrometers in diameter<sup>16</sup>) than bubbles generated in capillaries for two bubble interaction experiments or by gas extruded into a liquid through porous frits (millimeter scale). They have a rapidly changing interfacial area and perhaps most noteworthy is that they are relatively short-lived (sub-millisecond times), disappearing through either fragmentation, coalescence, or dissolution.<sup>15–19</sup>

The present study examines the coalescence of transient and highly dynamic bubbles as a new means of probing the origin of electrolyte effects on bubble coalescence. Coalescence behavior has been measured in aqueous solutions containing electrolytes that have shown coalescence inhibition of regular bubbles (MgSO<sub>4</sub>, NaCl, KCl) and those that have shown no effect (HCl, H<sub>2</sub>SO<sub>4</sub>). Also, the saturating gas has been varied (helium, argon, and air) to explore the role of this parameter in bubble coalescence.

## EXPERIMENTAL DETAILS

**Materials.** All solutions were prepared with Milli-Q purified water (resistivity of 18.2 MΩ cm at 25 °C). Sodium chloride (99.9%, BDH), magnesium sulfate anhydrous (>99.5%, Sigma-Aldrich), and potassium chloride (99%, Chem. Supply) were all calcined at 500 °C for 4 h to remove possible organic impurities and stored in a vacuum desiccator until required. Hydrochloric (37% RG), sulfuric (97% RG), and nitric (69% trace analysis grade) acids were supplied by Scharlau and used as received. Sodium hydroxide was sourced from Chem. Supply. Ethanol (100%) was obtained from Chem. Supply; *n*-propanol (>99.8%) was purchased from Fluka; *n*-pentanol (>99%) was obtained from Sigma-Aldrich. High purity helium and argon were purchased from BOC gases.

**Coalescence Measurements.** The coalescence measurements were conducted with a dilatometer similar to one used in our previous studies.<sup>14,15,17</sup> The dilatometer consisted of two sections, a customized glass cell and a second part, attached to the glass cell via a flange, onto which a 25 cm glass capillary was glass-blown. The glass cell had an approximate volume of 320 mL, and the capillary (internal diameter of 0.9 mm) attachment had a total volume of 25 mL. An ELAC LVG-60 RF generator was used in conjunction with an ELAC Allied Signal plate transducer of diameter 54.5 mm. The frequency of the ultrasound delivered by the unit was 213 kHz for the salt solutions with a calorimetrically determined power of 19.5 W. For the alcohol solutions, the same system was used but with an ultrasound unit operating at 355 kHz.

**Atomic Force Microscopy (AFM) Measurements.** AFM direct force measurements between two bubbles were conducted with an Asylum MFP-3D atomic force microscope that was equipped with a linear variable differential transformer (LVDT) sensor in the Z-movement direction. The LVDT allows the cantilever Z-position to be directly detected during force measurements. Custom made rectangular silicon AFM cantilevers (450 × 50 × 3 μm<sup>3</sup>) had a circular gold disk (diameter = 45 μm, thickness ≈ 20 nm) placed ≈ 2 μm from the end by focused ion-beam deposition. The cantilever spring constants were determined by the Hutter and Bechhoeffer<sup>20</sup> method. The spring constants of the cantilevers used were in the range of 0.2–0.6 N/m.

Before beginning AFM measurements, all glass surfaces were washed separately in 10% Ajax detergent, then 10% nitric acid, and then 10% sodium hydroxide. Following each washing step, copious amounts of deionized water were used to rinse the glassware. For the argon bubble

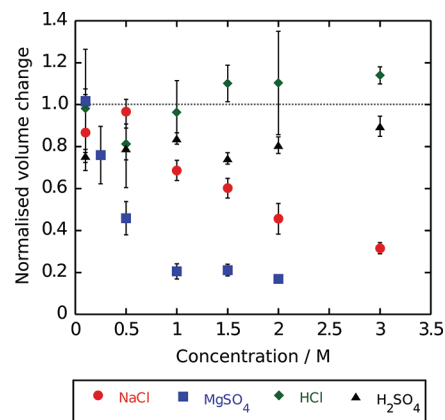


**Figure 1.** Normalized volume change for He saturated aqueous solutions of NaCl, MgSO<sub>4</sub>, HCl, and H<sub>2</sub>SO<sub>4</sub> as a function of electrolyte concentration. The volume change has been normalized against the measured value for pure water in He saturated solutions. The solutions were sonicated for 10 s at 213 kHz and 19.5 W. The rate of volume change in pure water was 3.5 μL/s.

experiments, the solutions were sparged with argon gas for 20 min prior to AFM measurements being conducted.

Bubbles were generated using an ultrasound transducer (Undatim Ultrasonics D-reactor) at a frequency of 515 kHz and power of 25 W within a glass Petri dish with a slightly hydrophobized surface.<sup>21</sup> The glass surface was washed utilizing the method above and hydrophobized through an esterification reaction in absolute ethanol for 2 h.<sup>22</sup> This reaction allows a surface that is hydrophobic enough for the generated bubbles to remain attached to the surface while also allowing them to be easily removed by the AFM cantilever. A single bubble was removed from the glass surface and anchored on the AFM cantilever. Another bubble of comparable size was located on the glass surface, and direct force measurements were conducted between the two bubbles. Experiments were arranged and observed using high-magnification optical microscopy from below (Nikon Ti-2000) to ensure an axisymmetric approach between the interacting bubbles.

## RESULTS AND DISCUSSION

The effect of electrolyte concentration, of several electrolytes, on the relative change in solution volume on sonication for helium, air, and argon saturated aqueous solutions is shown in Figures 1–3. In all the systems, the effect of the electrolytes on the volume change is in the order MgSO<sub>4</sub> > NaCl ≈ KCl > H<sub>2</sub>SO<sub>4</sub> ≈ HCl, with the latter two electrolytes showing almost no effect. Although, in the case of the argon system (Figure 3), there appears to be a slight inhibition effect from H<sub>2</sub>SO<sub>4</sub>.

A closer examination of the data in Figures 1–3 shows that the relative change in the solution volume as a function of electrolyte concentration for a specific electrolyte is approximately the same, irrespective of the gas type. This is shown for MgSO<sub>4</sub> in Figure 4. The plot is in the form typically used to arrive at a critical transition concentration ( $C_T$ ), taken to be the electrolyte concentration where the volume change is half of the value obtained in pure water. Based on this definition, the  $C_T$  values obtained from the present study are compared with values from other coalescence studies, for both acoustic and regular bubbles, in Table 1. Included in this table are  $C_T$  results obtained for aqueous solutions containing aliphatic alcohols in order to provide a broader base for interpreting the electrolyte results.

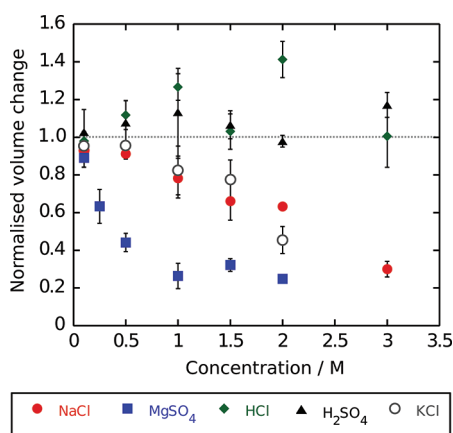


**Figure 2.** Normalized volume change for air saturated aqueous solutions of NaCl, MgSO<sub>4</sub>, HCl, H<sub>2</sub>SO<sub>4</sub>, and KCl as a function of electrolyte concentration. The volume change has been normalized against the measured value for pure water in air saturated solutions. The solutions were sonicated for 10 s at 213 kHz and 19.5 W. The rate of volume change in pure water was 3.7  $\mu\text{L}/\text{s}$ .

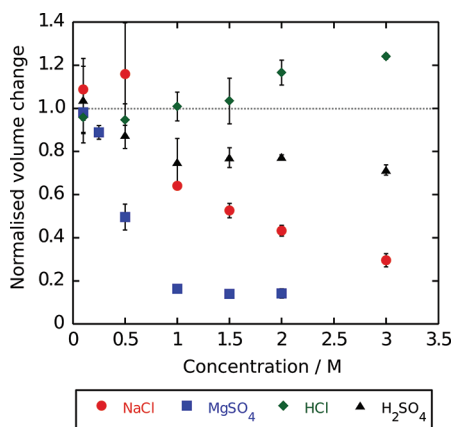


**Figure 3.** Normalized volume change for Ar saturated aqueous solutions of NaCl, MgSO<sub>4</sub>, HCl, and H<sub>2</sub>SO<sub>4</sub> as a function of electrolyte concentration. The volume change has been normalized against the measured value for pure water in argon saturated solutions. The solutions were sonicated for 10 s at 213 kHz and 19.5 W. The rate of volume change in pure water was 7.1  $\mu\text{L}/\text{s}$ .

The change in the solution volume on exposure to ultrasound is the result of a complex array of events.<sup>15,18</sup> From the onset of sonication, adventitious gas bubble nuclei in a fluid or on the walls of the vessel containing the fluid grow in size over a number of expansion and contraction cycles when acted on by an oscillating pressure field. The sound field also forces these growing bubbles to the antinodes, or nodes (depending on bubble size), that are established in these systems, where clusters of bubbles aggregate. It is within these bubble clusters (“clouds” of bubbles) that coalescence will occur. Bubbles of similar radii will synchronously oscillate and, if sufficiently close to each other, produce hydrodynamic flow conditions (secondary Bjerknes forces) that bring the bubbles together.<sup>11,24</sup>

In a bubble cloud, whether at the node or antinode, there will be a distribution of bubble sizes. Bubbles that reside in the core of a bubble cluster are likely to be shielded<sup>11</sup> from the sound field and not subject to secondary Bjerknes forces (for those at the antinode)

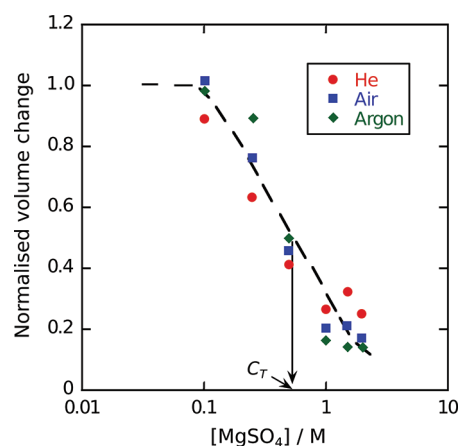


**Figure 4.** Comparison of the normalized volume changes on sonication of He, air, and Ar gas saturated aqueous solutions as a logarithmic function of the concentration of MgSO<sub>4</sub>. Data compiled from Figures 1–3.

but close enough together to be affected by electrostatic, steric, and van der Waals forces. In addition to these processes, some bubbles may also fragment during an oscillation cycle producing new bubble nuclei. Also, bubbles that do not experience an oscillating sound field (those at a node or within the core of a bubble cluster) will be inclined to dissolve, due to their intrinsic surface tension.

It is only the larger bubbles in the system, probably produced from multiple coalescence events of many smaller bubbles, that will have an extended persistence time, and it is these that are responsible for the volume change measured in Figures 1–3. Considering that the volume change remains constant for at least 1 min after sonication is stopped, the majority of the residual bubbles must be greater than 25  $\mu\text{m}$  in size. (A free bubble of radius 25  $\mu\text{m}$  takes about 70 s to dissolve in air-saturated water.<sup>25</sup>)

It is known that bubbles are charged in water and that the charge is dependent on the pH of the solution.<sup>26,27</sup> The presence of a charged interface will mean that there will be an increasing electrostatic repulsion between bubbles as they approach and this can be expected to affect bubble–bubble coalescence rates. Therefore, the effect of pH on bubble coalescence was examined, at both high and low pH, under ionic strength conditions where no coalescence inhibition was observed for the above electrolytes. The results shown in Figure 5 for air-saturated solutions clearly indicate solution pH does not affect the coalescence rate of acoustic bubbles.

Finally, in order to gauge the significance of the forces of interaction between two bubbles in the absence and presence of electrolyte, direct forces of interaction on approach of two,  $\sim 100 \mu\text{m}$  diameter argon bubbles, were determined; the results are presented in Figure 6. The data reveal that in pure water there is a significant electrostatic repulsive barrier generated as the two bubbles approach one another, and this prevents coalescence from occurring. However, once electrolyte is present in solution, at even relatively modest levels, the electrostatic repulsive barrier is greatly reduced and “jump-in” occurs, and bubble coalescence takes place. It can be noted that the electrolyte concentrations (apart from the 2 M MgSO<sub>4</sub>) used in the direct force experiments are of a level that were found not to affect the coalescence behavior of acoustic bubbles (e.g., see Figure 3). It should also be noted that the approach speed used for obtaining the results of Figure 6 was sufficiently slow in order to avoid hydrodynamic forces<sup>28,29</sup> due to film drainage between colliding bubbles.

**Table 1. Comparison of Bubble Coalescence Critical Transition Concentrations ( $C_T/M$ ) in Aqueous Solutions of Various Electrolytes and Aliphatic Alcohols**

solute	this study (213 kHz) <sup>a</sup>	Lee et al. (515 kHz) <sup>b</sup>	Sunartio et al. (358 kHz) <sup>c</sup>	Brotchie et al. (515 kHz) <sup>d</sup>	Oolman and Blanch <sup>e</sup>	Craig et al. <sup>f</sup>	Drogaris and Weiland <sup>g</sup>	Christenson et al. <sup>h</sup>
MgSO <sub>4</sub>	0.5	*		*	0.032	0.020		0.036
KCl	2.1	*		2.1	0.23; 0.20	0.120		*
NaCl	2.0	1.4		2.2	0.17	0.078		0.21
HCl	>3.5	*		>3	*	no transition		*
NaClO <sub>4</sub>	*	*		2.7	*	no transition		1.7
NaNO <sub>3</sub>	*	*		2.7	*	0.10		*
H <sub>2</sub> SO <sub>4</sub>	>3.5	*		*	*	no transition		*
methanol	*	0.4	*		1.8		*	
ethanol	0.06	0.05	0.06		0.14		*	
n-propanol	0.02	0.02	0.018		*		0.03	
n-butanol	*	*	0.004		0.0018		0.004	
n-pentanol	0.001	*	0.001		0.00021		0.0009	

<sup>a</sup>The alcohol results were at a frequency of 355 kHz. <sup>b</sup>Reference 14. <sup>c</sup>Reference 15. <sup>d</sup>Reference 17. <sup>e</sup>Reference 3 (some of the data quoted in this paper are taken from refs 1 and 2). <sup>f</sup>Reference 4. <sup>g</sup>Reference 23 [averaged values from data given]. <sup>h</sup>Reference 7. \*Represents no data available.

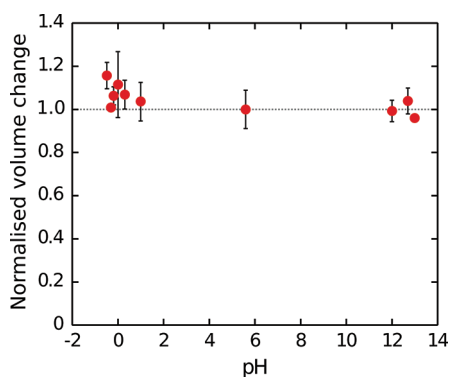


**Figure 5.** Normalized volume change of solutions in air at varying pH. The pH of pure water was measured at 5.6. The solutions were sonicated at 213 kHz and 19.5 W for 10 s. The rate of volume change for pure water was 3.7 mL/s.

In comparison, the presence of *n*-butanol in solution does not affect the electrostatic interaction between bubbles (see Figure 7). The contrast in behavior between the two solute types is typical of the electrostatic screening effects from electrolytes in the one case, and the neutral electrostatic influence of nonelectrolytes (alcohols) at the concentrations used in the experiments. For an *n*-butanol concentration of 500 mM, the adsorption density of an alcohol molecule at the bubble–solution interface should be approximately 5.9  $\mu\text{mol}/\text{m}^2$  (area per molecule of about 28  $\text{\AA}^2$ ).<sup>30</sup> This is only about 60% of monolayer coverage<sup>30</sup> of the surface and explains why there is little effect on the surface charge responsible for the electrostatic repulsion between the bubbles when alcohols are adsorbed to the bubbles solution interface. This surface charge however can be neutralized by  $\text{H}^+$  and hence the change in the interaction curves shown in Figure 7. (The change in the slope of the interaction curves in the presence of *n*-butanol is a consequence of the accompanying decrease in the surface tension of the air–solution interface.<sup>21,30</sup>)

Based on the data of Figures 1–4, it is evident that electrolytes, to varying extents, impart an effect that can on first inspection be interpreted as an inhibition of coalescence of acoustic bubbles.

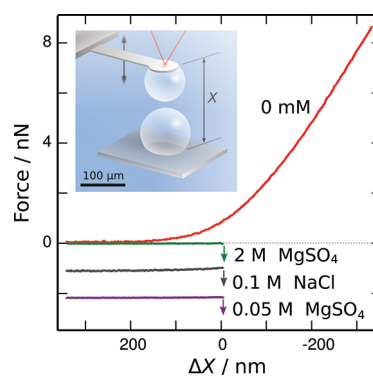


**Figure 6.** Direct force measurements between two argon bubbles in water at pH = 7; 50 mM and 2 M MgSO<sub>4</sub> solutions at pH = 7; 100 mM NaCl at pH = 7. An approach speed of 0.2 mm/s was used. The arrows indicate where “jump in” (coalescence) has occurred. The force curves for the electrolyte solutions have been offset for clarity.  $\Delta X$  represents the change in separation between the free end of the cantilever and the base on which the bottom bubble sits. The inset illustrates the AFM bubble–bubble arrangement used in the experiments and is also relevant to Figure 7.

However, critical transition concentrations listed in Table 1 for acoustic bubbles are some 10–25 times larger than those obtained by the other two techniques listed. The same is not the case for the alcohol systems where there is a much closer correspondence, both in trend and value (except perhaps for methanol), between the acoustic and nonacoustic derived  $C_T$  values. In fact, considering the vastly different methods used to measure the bubble coalescence process, the agreement in the  $C_T$  values can be considered very good.

Previous studies on acoustic bubbles in aqueous alcohol and surfactant solutions have shown that there is a strong correlation between the adsorption of solutes to the bubble–solution interface and the degree of coalescence inhibition.<sup>14,15</sup> This can also be inferred qualitatively from the observed decrease in  $C_T$  as the alkyl chain length of the alcohols increase from C1 to C5 shown in Table 1. A possible mechanism for this alcohol induced coalescence inhibition has been suggested to be due to short-range

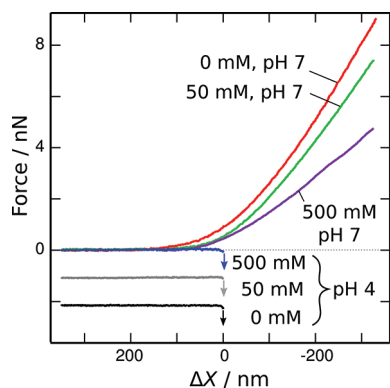


**Figure 7.** Direct force measurements between two air bubbles in water and 50 and 500 mM *n*-butanol solutions at pH = 7 and 4. An approach speed of 0.2 mm/s was used. The arrows indicate where “jump in” (coalescence) has occurred. The force curves for the solutions at pH = 4 have been offset for clarity. The  $\Delta X$  represents the change in separation between the free end of the cantilever and the base on which the bottom bubble sits.

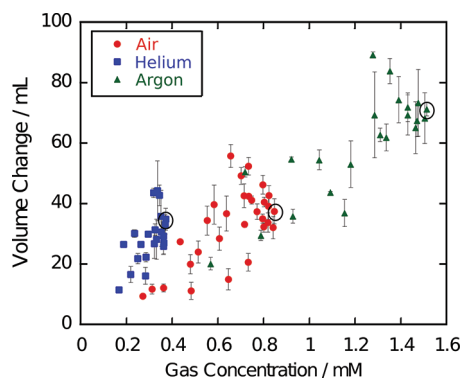


**Figure 8.** Volume change of all solutions, salt types, and concentrations from Figures 1–3 as a function of saturating gas concentration. The values for pure water saturated with He, air, and Ar are circled. The volume changes were recorded after the solutions were sonicated for 10 s at 213 kHz and 19.5 W. (The experimental conditions used are such that ultrasonic degassing is not significant.<sup>14,31</sup> Gas solubilities are taken from literature sources.<sup>32–38</sup>)

steric hindrance from interfacially adsorbed alcohol.<sup>15</sup> However, it is important at this point to note that direct force measurements between bubbles in solutions containing *n*-butanol (50 and 500 mM in Figure 7) at pH = 4 (the iep<sup>27</sup>) show no difference to the alcohol free bubble–bubble interactions, and there is no suggestion at all of any short-range repulsive force.

In order to rationalize the relative volume changes measured in Figures 1–3, in view of the observations made above, it is relevant to consider gas solubility in the various aqueous electrolyte solutions, that is, the gas “salting out” properties of the electrolytes. Figure 8 shows a composite of all the volume change data as a function of the equilibrium gas solubility in all the aqueous electrolyte solutions. The results show a linear correlation between the volume change recorded and the gas content of the solutions. There are no obvious specific ion effects. Furthermore, it has been previously noted that degassing water can generate the same effect.<sup>14</sup> The simplest interpretation then of the results in Figures 1–4 is that the number of stable bubbles, hence the total volume change, produced through the coalescence of smaller

bubbles decreases as the gas content of the aqueous solution decreases. That is, the lower gas content in solution reduces the total volume of precursors gas nuclei that lead to the stable final bubbles.

Although the above explanation is able to account for the trend seen in Figure 8, it does not explain why there are no specific ion effects in play in acoustic bubble coalescence processes. Nor does it explain why there is no effect of bubble surface charge/electrostatics when there are distinct changes in the bubble–bubble interaction forces with pH and ionic strength changes. Both these observations can be addressed through a consideration of the dynamic properties of acoustic bubbles and other kinetic processes in play in such systems.

Brothie and co-workers<sup>17,19</sup> have already made the point that acoustic bubbles experience a relatively rapid process of volume expansion from isolated gas nuclei to clusters of high volume fraction, and to then dissipate through coalescence and other paths, all within 0.5 ms. Over this time frame, it would appear that short chain aliphatic molecules are able to adsorb to acoustic bubbles to impart their influence on the coalescence process.<sup>14,15</sup> This is quite consistent with kinetic studies of alcohol adsorption to an air–water interface, showing adsorption is diffusion controlled;<sup>39</sup> at the concentrations used in the acoustic bubble coalescence measurements, almost complete interfacial adsorption would occur on a sub-millisecond to millisecond time scale.<sup>39</sup> If the premise is accepted that interfacial ion adsorption is behind the coalescence inhibition effect for electrolytes, it can be inferred that ions cannot adsorb to the bubble–solution interface at sub-millisecond times. There is some support for this conclusion in the work of Kochurova and Rusanova who have reported on the equilibration time of a freshly created air–water interface.<sup>40</sup> They show that the surface tension (strictly, a dynamic surface tension) of water changes from 180 mN/m to its equilibrium value of 72 mN/m at 25 °C, in about 3 ms. They speculate that this change is associated with changes in the net orientation of interfacial water molecules over this time. However, as Beattie<sup>41</sup> has suggested, it may represent the process of hydroxide ion adsorption.

If it is the case that ion equilibration with a bubble–solution interface is slower than on a millisecond time scale, it would also mean that the equilibrium force measurements (Figures 6 and 7) are not a true representation of the electrostatic interactions between acoustic bubbles over a sub-millisecond time frame. That is, the repulsive interactions between bubbles as measured by the AFM would not be reflective of the “naked” air–water interface at sub-millisecond times. This would explain the lack of a pH effect (Figure 5) in the coalescence of acoustic bubbles. Also, considering the time scale (fractions of a second to around 1 s) over which bubble interactions occur in those experiments that show electrolyte induced coalescence impedance,<sup>1–4,7</sup> it can be deduced that the ion adsorption process is likely to be on a millisecond time scale, perhaps hundreds of milliseconds, for equilibration with the gas–solution interface to be achieved.

It is also relevant to comment on the importance of bubble oscillations in the inhibition to coalescence. All bubbles have an intrinsic oscillation frequency ( $\nu_o$ ) given by the Minnaert equation,<sup>11</sup>  $\nu_o R_o \cong 3$  (m/s). Bubbles of 2  $\mu\text{m}$  radius ( $R_o$ ), which is typical of transient acoustic bubbles,<sup>16</sup> oscillate at 1.5 MHz, with an amplitude of a few angstroms at room temperature. The action of an applied sound field is to perturb this natural oscillation and to cause the bubble to oscillate at a frequency closer to the frequency of the impinging sound wave. In the present study, this

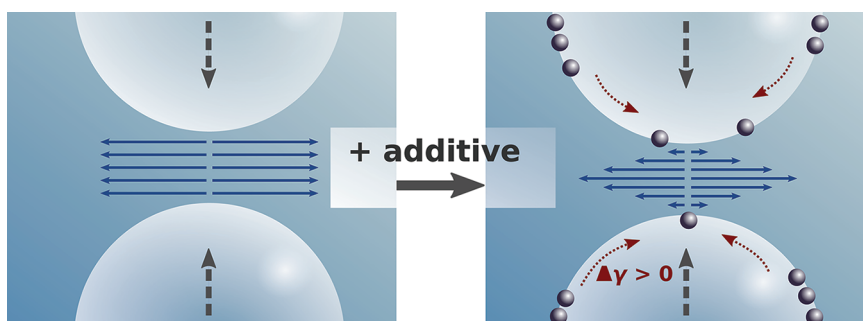


**Figure 9.** Stylized diagram illustrating the change in fluid flow in a film between two colliding air bubbles in solution before and after adsorption of a surface-active additive at a level that converts the fluid flow near a surface from mobile to completely tangentially immobile. Surface tension gradients ( $\Delta\gamma > 0$ ) are present due to the nonuniform distribution of the adsorbed solute at the bubble surface. (Bubble and film dimensions are not drawn to scale.)

frequency is 213 kHz, resulting in oscillation amplitudes on the micrometer scale.<sup>11</sup> If interfacial oscillations alone were important in the bubble coalescence process, one would expect a significant change in the  $C_T$  values for the different frequencies listed in Table 1. This is clearly not the case.

In comparing the electrolyte results with the alcohol systems and taking into account the comments above, it is reasonable to conclude that, for the rate of bubble coalescence to be impeded, solute adsorption onto the gas–solution interface must take place. Once this adsorption has occurred, another process must come into play that retards the film drainage between the colliding bubbles. Electrostatic interactions, counterintuitively, do not seem to be a significant factor in retarding the film drainage process. This can be concluded from the similarity of the alcohol  $C_T$  values of acoustic bubbles and the nonacoustic bubbles; perhaps more significantly, alcohols inhibit coalescence but have no effect on the strong electrostatic interaction between bubbles (see Figure 7). It would seem that either adsorbed ions (or ion-pairs, more will be said on this later) or neutral molecules are able to establish the conditions that inhibit the rate of film thinning between colliding bubbles.

The simplest conceptual model that can unite all the above observations is one where the adsorbed material converts a bubble–solution interface, in-so-far as its hydrodynamic behavior is concerned, from a tangentially mobile interface that cannot support a tangential stress to one that is tangentially immobile and behaves like a solid–liquid interface. Levich<sup>42</sup> introduced a theoretical model where the presence of trace amounts of unevenly distributed solute at a bubble–solution interface can give rise to a tangential surface tension gradient and, hence, a tangential stress (Marangoni stress) that opposes a flow shear stress. The motion of the flow of fluid in a film near such a surface is thus retarded and experiences a drag force similar to that near a solid sphere. Figure 9 schematically depicts this transition. The significance of this interpretation is that all  $C_T$  values, irrespective of the solutes involved, are effectively the critical concentrations in the conversion from the tangentially mobile condition of a “clean” interface to a tangentially immobile state, rendered so by the effect of spatially nonuniform adsorption of solute at the bubble–solution interface. Interestingly, for electrolyte systems, this suggestion has been previously proposed by Henry and Craig,<sup>43</sup> based on their study of bubble coalescence in nonaqueous electrolyte solutions. However, in the same year, they concluded that this hypothesis was not supported considering the results of bubble rise experiments in aqueous electrolyte solutions.<sup>44</sup> In view of the present results that indicate that

quantitative ion adsorption onto an air–solution interface is likely to be on a many milliseconds to a second time scale, the conclusions drawn from the latter study<sup>44</sup> appear not to be valid. This can be further qualified by the bubble rise experiments reported by Malysa et al.<sup>45</sup> These authors found that even in aqueous solutions containing a surface active solute, a fresh bubble may first behave with a mobile interface, reach terminal velocity, and then reduce its rise velocity to a level consistent with an immobile interface. For example, a rising bubble in 5 mM *n*-butanol ( $C_T$  of around 4 mM), after establishing a terminal velocity consistent with a mobile interface, requires about 0.7 s to fully establish a velocity comparable to a bubble possessing an immobile interface.

There are several observations that can be made to support the above interpretation. Chan and co-workers<sup>46</sup> have theoretically considered the conditions needed at a bubble–solution interface to move from a mobile to an immobile boundary condition. They show that adsorption of a solute need only induce an interfacial tension gradient of as little as 0.1–1 mN/m for the transition to take effect. An examination of the surface tensions<sup>47</sup> of the *n*-alcohols at the concentrations at which the  $C_T$  values are measured shows that they impart a surface tension change of less than 1 mN/m to the air–solution interface. Alternatively, using the data from Sunartio et al.,<sup>15</sup> an upper estimate of a few percent of monolayer coverage, irrespective of the alcohol, can be estimated. (This is using an *n*-alcohol cross-sectional size of 18.4 Å<sup>2</sup>/molecule.<sup>30</sup>) Experimental evidence that trace levels of surface active solute adsorption to an air bubble–solution interface converts a mobile interface into an immobile one is also obtained in rising bubble measurements.<sup>47,48</sup> All this indicates that relatively small amounts of adsorbed material are required to achieve a significant change in the flow conditions that exist near the surfaces of approaching bubbles.

For the case of electrolytes, it is tempting, based on the above discussion, to attribute the  $C_T$  to adsorption of individual ions to the interface, again leading to conditions that produce an immobilized flow at the surface. There is a growing body of work<sup>49–52</sup> that appears to indicate ion adsorption at air–water interfaces does occur and would support such an assignment. However, that alone is not sufficient to fully explain the experimental results that show that it is a certain mix of cation–anion couples<sup>4,8</sup> that causes the transition effect.

An alternative to specific ion adsorption, but incorporating the empirically observed ion couple effects on  $C_T$ , would be the case where the entity adsorbed at the interface was an ion-pair complex, as distinct to ion couples at different locations (surface/subsurface)

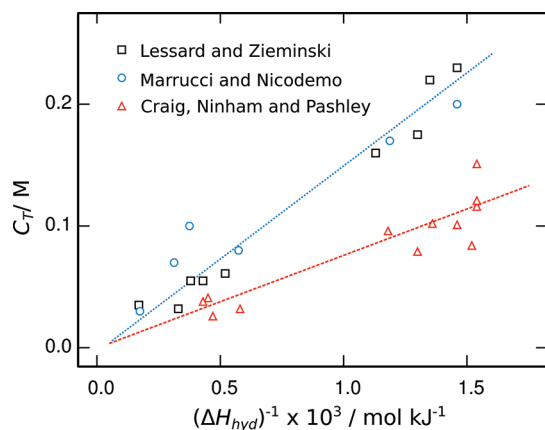


**Figure 10.** Critical transition concentration as a function of the reciprocal of the sum of cation and anion hydration enthalpies.<sup>55,56</sup> Two sets of data are shown for  $C_T$  values taken from refs 1, 2, and 4. The differences in the two sets of  $C_T$  values probably reflect the quite different techniques (and, hence, perhaps time scales) used to make the relative coalescence measurements.

at an interface.<sup>8</sup> Ion-pair complexes of simple ions are not normally present in water, but as the interface provides a lower dielectric environment,<sup>53,54</sup> it may be the situation that these types of complexes are stabilized under such conditions. It is difficult to prove such a suggestion, as the quantities, as already explained, can be expected to be very low, and it would be difficult to experimentally distinguish between an ion-pair complex and background hydrated ions near an interface, considering the high electrolyte concentrations that induce the  $C_T$ . Indirect evidence that ion-pair complexes are the likely adsorbing species is given in Figure 10. The main contributor to the  $\Delta H_{\text{hyd}}$  term is the cation. The correlation observed in Figure 10 would suggest that, for strongly hydrated cations (that have the greatest influence on  $C_T$ ) to exist in a low dielectric environment, an accompanying electrostatically neutralizing anion would have to be present, that is, an ion-pair complex. Also, it is energetically highly unfavorable for a formally charged species to move from a high dielectric constant medium to a low dielectric medium unless accompanied by a counter charge, just what an ion-pair complex achieves. Stated in another way, the trend of lowering of  $C_T$  with increasing hydration energy of the ions is a reflection of the ion-pair complex formed at the bubble surface in order to achieve the change in the shear flow conditions at a bubble–solution interface. It now behooves the experimentalists to verify this proposition.

## SUMMARY AND CONCLUSIONS

The present study has attempted to integrate bubble coalescence data in aqueous electrolyte and alcohol solutions from several sources that have used quite different experimental techniques. It is shown that neither gas type (air, Ar, He) nor colloidal forces, as measured using direct AFM force measurements between two bubbles, play a significant role in bubble coalescence inhibition by ions and alcohols. The comparison of acoustic bubble coalescence impedance rates with those under “silent” conditions in aqueous electrolyte and alcohol solutions strongly suggests that the critical transition concentration,  $C_T$ , widely reported for electrolytes and other solutes, identifies a solute induced change in the hydrodynamic boundary conditions at the bubble–solution interface. The “transition” is brought

about through the adsorption of solute at trace levels to the interface in a spatially nonuniform distribution; this gives rise to surface tension gradients that render the interface tangentially immobile. This condition has a strong effect on the film drainage rate between the bubbles and hence their coalescence rate. In electrolyte solutions, the solute responsible is suggested to be an overall electrostatically neutral cation–anion ion-pair complex. It is also concluded that the ion adsorption process at the bubble–solution interface is not diffusion controlled and probably requires fractions of a second in order to be established.

## AUTHOR INFORMATION

### Corresponding Author

\*E-mail: franz@unimelb.edu.au.

## ACKNOWLEDGMENT

We thank Jim Beattie (University of Sydney) for drawing our attention to ref 40. Funding for this work was provided by the Australian Research Council.

## REFERENCES

- (1) Marrucci, G.; Nicodemo, L. *Chem. Eng. Sci.* **1967**, *22*, 1257–65.
- (2) Lessard, R. R.; Zieminski, S. A. *Ind. Eng. Chem. Fundam.* **1971**, *10*, 260–269.
- (3) Oolman, T. O.; Blanch, H. W. *Chem. Eng. Commun.* **1986**, *43*, 237–261.
- (4) Craig, V. S. J.; Ninham, B. W.; Pashley, R. M. *J. Phys. Chem.* **1993**, *97*, 10192–10197.
- (5) Weissenborn, P. K.; Pugh, R. J. *Langmuir* **1995**, *11*, 1422–1426.
- (6) Christenson, H. K.; Yaminsky, V. V. *J. Phys. Chem.* **1995**, *99*, 10420.
- (7) Christenson, H. K.; Bowen, R. E.; Carlton, J. A.; Denne, J. R. M.; Lu, Y. *J. Phys. Chem. C* **2008**, *112*, 794–796.
- (8) Henry, C. L.; Craig, V. S. J. *Langmuir* **2010**, *26*, 6478–6483.
- (9) Craig, V. S. J. *Curr. Opin. Colloid Interface Sci.* **2011**, published online May 8, DOI:10.1016/j.cocis.2011.04.003
- (10) Horn, R. G.; Del Castillo, L. A.; Ohnishi, S. *Adv. Colloid Interface Sci.* **2011**, published online May 19, DOI:10.1016/j.cis.2011.05.006
- (11) Leighton, T. G. *The Acoustic Bubble*; Academic Press: London, 1994.
- (12) Appel, J.; Koch, P.; Mettin, R.; Krefting, D.; Lauterborn, W. *Ultrason. Sonochem.* **2004**, *11*, 29–42.
- (13) Crum, L. A.; Mason, T. J.; Reisse, J. L.; Suslick, K. S., Eds. *Sonochemistry and Sonoluminescence. NATO ASCI Series C: Mathematical and Physical Sciences*; Kluwer Academic Publishers: The Netherlands, 1999; Vol. 524.
- (14) Lee, J.; Kentish, S. E.; Ashokkumar, M. *J. Phys. Chem. B* **2005**, *109*, 5095–5099.
- (15) Sunartio, D.; Ashokkumar, M.; Grieser, F. *J. Am. Chem. Soc.* **2007**, *129*, 6031–6036.
- (16) Brotchie, A.; Grieser, F.; Ashokkumar, M. *Phys. Rev. Lett.* **2009**, *102*, 084302.
- (17) Brotchie, A.; Stratham, T.; Zhou, M.; Dharmarathne, L.; Grieser, F.; Ashokkumar, M. *Langmuir* **2010**, *26*, 12690–12695.
- (18) Iida, Y.; Ashokkumar, M.; Tuziuti, T.; Kozuka, T.; Yasui, K.; Towata, A.; Lee, J. *Ultrason. Sonochem.* **2010**, *17*, 480–486.
- (19) Brotchie, A.; Grieser, F.; Ashokkumar, M. *J. Phys. Chem. B* **2010**, *114*, 11010–11016.
- (20) Hutter, J. L.; Bechhoefer, J. *Rev. Sci. Instrum.* **1993**, *64*, 1868–1873.
- (21) Vakarelski, I. U.; Lee, J.; Dagastine, R. R.; Chan, D. Y. C.; Stevens, G. W.; Grieser, F. *Langmuir* **2008**, *24*, 603–605.
- (22) Biggs, S.; Grieser, F. *J. Colloid Interface Sci.* **1994**, *165*, 425–430.

- (23) Drogaris, G.; Weiland, P. *Chem. Eng. Sci.* **1983**, *38*, 1501–1506.
- (24) Segabarth, N.; Eularths, O.; Reisse, J.; Crum, L. A.; Matula, T. J. *J. Phys. Chem. B* **2002**, *106*, 9181–9190.
- (25) Epstein, P. S.; Plesset, M. S. *J. Chem. Phys.* **1950**, *18*, 1505–1509.
- (26) Creux, P.; Lachaise, J.; Graciaa, A.; Beattie, J. K.; Djerdjev, A. M. *J. Phys. Chem. B* **2009**, *113*, 14146–14150.
- (27) Tabor, R. F.; Chan, D. Y. C.; Grieser, F.; Dagastine, R. R. *Angew. Chem., Int. Ed.* **2011**, *50*, 3454–3456.
- (28) Dagastine, R. R.; Manica, R.; Carnie, S. L.; Chan, D. Y. C.; Stevens, G. W.; Grieser, F. *Science* **2006**, *313*, 210–213.
- (29) Vakarelski, I. U.; Manica, R.; Tang, X.; O'Shea, S. J.; Stevens, G. W.; Grieser, F.; Dagastine, R. R.; Chan, D. Y. C. *Proc. Nat. Acad. Sci. U.S.A.* **2010**, *107*, 11177–11182.
- (30) Kipling, J. J. *J. Colloid Sci.* **1963**, *18*, 502–511.
- (31) Henglein, A.; Herburger, D.; Gutierrez, M. *J. Phys. Chem.* **1992**, *97*, 1126–1130.
- (32) Pawlikowski, E. M.; Prausnitz, J. M. *Ind. Eng. Chem. Fundam.* **1983**, *22*, 86–90.
- (33) Narita, E.; Lawson, F.; Han, K. N. *Hydrometallurgy* **1983**, *10*, 21–37.
- (34) Battino, R.; Rettich, T. R.; Tominaga, T. *J. Phys. Chem. Ref. Data* **1983**, *12*, 163–178.
- (35) Battino, R.; Rettich, T. R.; Tominaga, T. *J. Phys. Chem. Ref. Data* **1984**, *13*, 563–600.
- (36) Tromans, D. *Hydrometallurgy* **1998**, *50*, 279–296.
- (37) Clever, H. L.; Holland, C. J. *J. Chem. Eng. Data* **1968**, *13*, 411–414.
- (38) Morrison, T. J.; Johnstone, N. B. *J. Chem. Soc.* **1955**, 3655–3659.
- (39) Fainerman, V. B.; Miller, R. *J. Colloid Interface Sci.* **1996**, *178*, 168–175.
- (40) Kochurova, N. N.; Rusanova, I. *J. Colloid Interface Sci.* **1981**, *81*, 297–303.
- (41) Beattie, J. Personal communication.
- (42) Levich, V. G. *Physicochemical hydrodynamics*; Prentice Hall: Englewood Cliffs, NJ, 1962.
- (43) Henry, C. L.; Craig, V. S. *J. Langmuir* **2008**, *24*, 7979–7985.
- (44) Henry, C. L.; Parkinson, L.; Ralston, J. R.; Craig, V. S. *J. Phys. Chem. C* **2008**, *112*, 15094–15097.
- (45) Malysa, K.; Krasowska, M.; Krzan, M. *Adv. Colloid Interface Sci.* **2005**, *114–115*, 205–225.
- (46) Manor, O.; Vakarelski, I. U.; Stevens, G. W.; Grieser, F.; Dagastine, R. R.; Chan, D. Y. C. *Langmuir* **2008**, *24*, 11533–11543.
- (47) Shaw, D. J. *Introduction to Colloid and Surface Chemistry*, 4th ed.; Butterworth-Heinemann: Oxford, 1992; p 78.
- (48) Clift, R.; Grace, J.; Weber, M. E. *Bubbles, Drops and Particles*; Dover Publications Inc.: Mineola, NY, 2005.
- (49) Kunz, W., Ed. *Specific Ion Effects*; World Scientific Publishing Co.: Singapore, 2010.
- (50) Manciu, M.; Ruckenstein, E. *Adv. Colloid Interface Sci.* **2003**, *105*, 63–101.
- (51) Baer, M. D.; Kuo, I-F. W.; Bluhm, H.; Ghosal, S. *J. Phys. Chem. B* **2009**, *113*, 15843–15850.
- (52) Raymond, E. A.; Richmond, G. L. *J. Phys. Chem. B* **2004**, *108*, 5051–5059.
- (53) Grieser, F.; Thistlethwaite, P. J.; Triandos, P. *J. Am. Chem. Soc.* **1986**, *108*, 3844–3846.
- (54) Lima, E. R. A.; Horinek, D.; Netz, R. R.; Biscaia, E. C.; Tavares, F. W.; Kunz, W.; Boström, M. *J. Phys. Chem. B* **2008**, *112*, 1580–1585.
- (55) Dasent, W. E. *Inorganic Energetics: An Introduction*, 2nd ed.; Cambridge University Press: Cambridge, U.K., 1982.
- (56) Smith, D. W. *J. Chem. Educ.* **1977**, *54*, 540–542.